DOI 10.1007/s11182-017-1011-0

Russian Physics Journal, Vol. 59, No. 12, April, 2017 (Russian Original No. 12, December, 2016)

STATISTICAL ESTIMATES OF LIDAR SIGNALS REFLECTED FROM THE OCEAN BOTTOM

V. S. Shamanaev,[1] A. I. Potekaev,[2,3] A. A. Lisenko,[1] and M. G. Krekov[2]

UDC 551.46.07

The Monte Carlo method is used to solve the nonstationary equation of laser sensing of an optically dense, complex, multicomponent aqueous medium with allowance for the water–air interface, the contribution of multiple scattering of radiation by the water column, and reflection of the signal from the bottom. As a result, we have obtained dependences of the return signal of a monostatic lidar from the water column and the surface microwaves for various field-of-view angles of the receiver. The results of our calculations show that a lidar detection depth of the bottom up to 50 m is achievable for water optical thicknesses up to 3.5–4. When sensing the bottom up to the limiting depth of 50 m under conditions of very transparent water and Fresnel reflection from its surface, the dynamic range of the signal from the water column reaches 7–9 orders of magnitude.

Keywords: lidar, ocean optics, multiple scattering of light, ocean depth.

INTRODUCTION

The first lidar measurements of ocean depth [1–3] made clear the need to overcome difficulties in the recording and interpretation of signals, the main ones of which are connected with water turbidity [4, 5] and the need for high temporal resolution [6, 7]. The range of laser wavelengths suitable for sensing the water column is limited to the blue-green region of the spectrum. The lasers should be pulsed and operate in the nanosecond range of pulse widths. In the measurement of the depth, special attention must be given to Fresnel reflection of laser radiation from the sea surface and to multiple scattering of light. In this regard, it has been theoretically and experimentally shown that the optical depth τ from the sea surface to the ocean bottom should not exceed $\tau = 3.75–4.0$ [8]. This limitation is connected with the dynamic range of the received signal [9].

The available analytical approximations for solutions of the radiative transfer equation are not able to reconstruct the full picture of the formation of the reflected light field, taking into account all of the above-enumerated factors. The only possibility of taking the complex picture of interaction of radiation with a scattering and reflecting medium into account is a statistical approach to the solution of the equation of radiative transfer [10].

In the present work we investigate the dependences of the return signal of a monostatic lidar on ocean depth for various field-of-view angles of the receiver. We use the Monte Carlo method to solve the nonstationary equation of transfer of laser radiation in sea water with allowance for the influence of the air–water interface, the contribution of multiple scattering, and Lambertian reflection from the ocean bottom.

[1]V. E. Zuev Institute of Atmospheric Optics of the Siberian Branch of the Russian Academy of Sciences, Tomsk, Russia, e-mail: shvs@iao.ru; Lisenko@iao.ru; [2]National Research Tomsk State University, Tomsk, Russia; [3]V. D. Kuznetsov Siberian Physical-Technical Institute at Tomsk State University, Tomsk, Russia, e-mail: kanc@spti.tsu.ru. Translated from Izvestiya Vysshikh Uchebnykh Zavedenii, Fizika, No. 12, pp. 51–56, December, 2016. Original article submitted June 17, 2016.

MODELS AND APPROXIMATIONS

Let a monostatic lidar be located at an altitude h above the sea surface. We assume that the laser radiation is directed vertically downward, passes through the *air–water* interface, is absorbed and scattered in the water column, is reflected from the ocean bottom, and is received by the detector. In sensing of a scattering medium, the single-scattered signal in the direction of the optical detector is considered as the carrier of useful information and is described mathematically by the canonical equation

$$P_{\text{bs}}(h) = W_0 A \sigma_\pi(h) h^{-2} \exp\left\{-2\int_0^h \sigma(h)\,dh\right\}, \tag{1}$$

where $P_{\text{bs}}(h)$ is the recorded signal, W_0 is the energy of the light pulse, A is the instrument function, and $\sigma_\pi(h)$ and $\sigma(h)$ are the volume coefficients of backscattering and attenuation.

The laser radar (lidar) signal is defined in terms of the following additive terms:

$$P(h) = P_{\text{bs}}(h) + P_{\text{bg}}(h) + P_{\text{surf}}(h),$$

where $P_{\text{bs}}(h)$ is the signal due to backscattering from aerosol and hydrosol and molecular scattering of pure water, $P_{\text{bg}}(h)$ is the multiple scattering background, and $P_{\text{surf}}(h)$ is the signal component due to reflection from the sea surface.

In the modeling of the lidar system, the estimate of the recorded signal $P(h)$ given by the single-scattering component $P_{\text{bs}}(h)$ (expression (1)) can in many cases be inadequate. More complete information about the energetic and temporal properties of the return signal $P(h)$ can be obtained by solving the nonstationary radiative transfer equation

$$\frac{\partial I(\boldsymbol{r},\boldsymbol{\Omega},t)}{\partial t} + \boldsymbol{\Omega}\nabla I(\boldsymbol{r},\boldsymbol{\Omega},t) = -\sigma(\boldsymbol{r})\left(I(\boldsymbol{r},\boldsymbol{\Omega},t) + \frac{1}{4\pi}\int d\boldsymbol{\Omega}' g(\boldsymbol{\Omega},\boldsymbol{\Omega}',\boldsymbol{r}) I(\boldsymbol{r},\boldsymbol{\Omega}',t)\right), \tag{2}$$

where $I(\boldsymbol{r},\boldsymbol{\Omega},t)$ is the radiative flux at the point of phase space $(\boldsymbol{r},\boldsymbol{\Omega},t)$, $\boldsymbol{r}$ is the radius vector representing the position of the photon, $\boldsymbol{\Omega}$ is the unit vector in the direction of motion of the photon, $\sigma(\boldsymbol{r})$ is the volume attenuation coefficient, $g(\boldsymbol{\Omega},\boldsymbol{\Omega}',\boldsymbol{r})$ is the scattering phase function, describing the scattering of the photons from the direction $\boldsymbol{\Omega}'$ into the direction $\boldsymbol{\Omega}$ in each scattering act.

In laser sensing of any scattering medium, the presence of a multiple scattering background inside the field-of-view cone of angles of the receiver is unavoidable. On the one hand, the multiple scattering background plays a negative role, increasing the error in the determination of the attenuation coefficient of the sea water. On the other hand, multiple scattering plays a positive role by raising the overall energetics of the sounding pulse.

To solve problems of radiative transfer under the complex boundary conditions of a field experiment, it is advantageous to use the Monte Carlo method. Without dwelling on the essence of the method, let us only note some characteristic aspects of the method that arise in its use. In the solution of this class of problems, use is most often made of the local estimation method [10]. The process of *wandering* of a photon in the medium is simulated, where at each collision point of the photon with a scattering particle the probability of incidence of the photon on the detector is estimated. This makes it possible to estimate with confidence the characteristics of the radiation field in fixed regions that are as small as desired. Using the local estimation approach, an analogous scheme for simulating the diffusion process is used, which involves averaging of a random quantity of the form [10]

$$\xi = \sum_{i=1}^{N_i} \frac{\omega_i \exp\{-\tau(\boldsymbol{r}_i,\boldsymbol{r}^*)\}\, g(\boldsymbol{\Omega}_i,\boldsymbol{\Omega}^*)}{|\boldsymbol{r}_i - \boldsymbol{r}^*|^2} \Delta(t_k)\Delta(\boldsymbol{\Omega}_m).$$

Here, the sought-after number of photons in the flux $I = \sum \xi_n \ (n = 1, 2, \ldots, N)$ is equal to the integral of the flux of scattered photons at the point $\boldsymbol{r}^* \in D$ over characteristic time intervals $\Delta t_k \ (k = 1, \ldots, n_k)$ and directions of approach of the photons $\Delta(\Omega_m)$, $m = 1, 2, \ldots, n_m$. Here ω_i is the conditional statistical weight of the photon in the *i*th collision of the *n*th trajectory, N_i is the number of informative collisions of the photon in the medium, N is the number of random trajectories, $g(\boldsymbol{\Omega}_i, \boldsymbol{\Omega}^*)$ is the scattering phase function, and $\tau(\boldsymbol{r}_i, \boldsymbol{r}^*)$ and $|\boldsymbol{r}_i - \boldsymbol{r}^*|$ are the optical path length and the geometrical path length from the collision point $\boldsymbol{r}_i$ to the point $\boldsymbol{r}^* \in D$ of the detector. A note about terminology is in order here. The scattering phase function is equal to (actually, is defined as) the volume scattering function $\beta(\varphi)$ normalized to *b*, the scattering coefficient, which is equal to its integral over all angles φ from 0 to π.

OPTICAL MODEL OF THE MEDIUM

Let us turn our attention to scattering phase functions with a strongly asymmetric shape for which the probability of scattering into the forward hemisphere with respect to motion of the photon significantly exceeds the probability of scattering in the backward direction (strongly forward peaked). As a result, the difference in variances of the estimates for the two types of trajectories can reach an order-of-magnitude value of ~10^4, in spite of the reciprocity theorem, from which it follows that these two estimates should be identical due to equivalence of the contributions to the sought-after functional from the two types of trajectories. Statistical overshoots of large magnitude appear; the bias grows upon taking into account large interaction multiplicities. The statistical validity of estimates of the second type of trajectories can be enhanced using importance sampling technique [10], which was in fact done in [11].

To simulate the lidar signal adequately, it is also necessary to take into account the component of the signal reflected from the sea surface, which is a specularly reflective surface. In addition, when sensing through the air–water interface, the laser beam splits in a random fashion into a set of beamlets (or rays) due to the presence of the wind-driven sea waves. A ray exiting the water is also split up in a random fashion with corresponding changes in its direction of propagation. As a result of these two processes, an increase in the above surface wind speeds leads to a reduction of the power level of the return signal reflected by the water column over the entire time interval of the return signal, and also to a reduction of the amplitude of the signal reflected from the bottom.

Moreover, when such a *split* laser beam is incident upon the sea bottom, its diameter is increased manyfold. For deviation of the beam from the vertical at the edge of the scanning line, the diameter of the spot on the bottom will be increased still more due to the laws of refraction. Of course, the brightness of such a spot will necessarily be nonuniform across its cross section. If the surface of the bottom at this level is not flat and consequently its albedo is nonconstant, errors will appear.

Of course, the wavy water surface will be one more source of errors. Whereas microwaves (millimeters and centimeters) will lead to splitting up of the beam, energetic waves (tens of centimeters) will pose the question as to what parameter of these waves will be used as a reference parameter for the measurements. Simulation of the effect of a wavy air–water interface can be performed with a high degree of confidence on the basis of the facet model [12–15], which treats the surface as a set of randomly oriented micropatches with centers in one horizontal plane. It assumes that the passage of radiation through each micropatch obeys the well-known Fresnel laws of reflection and refraction.

In accordance with the facet model, the normal vectors to the micropatches $S = (S_x, S_y, S_z)$ conform to a normal (Gaussian) distribution.

$$P(S) = P(\alpha_x, \alpha_y) = \frac{1}{2\pi\sigma_x\sigma_y} \exp\left\{-\frac{\alpha_x^2}{2\sigma_x^2} - \frac{\alpha_y^2}{2\sigma_y^2}\right\}, \tag{3}$$

where $\alpha_x = S_x/S_z$ and $\alpha_y = S_y/S_z$. The variances of the tilt angles change, depending on the wind speed *V*. The dependence that is usually used is [14]

$$\sigma_x^2 = 0.0031\ V,\ \sigma_y^2 = 0.003 + 0.00192\ V. \quad (4)$$

To solve the nonstationary equation of radiative transfer (Eq. (2)), it is unconditionally necessary to know the inherent optical characteristics (IOC) of the water. Their values at each wavelength depend only on the substances contained in the water, but do not depend on the conditions of illumination.

The main IOC in general use are the absorption coefficient a, the scattering coefficient b, and two quantities derived from them: the attenuation coefficient $c = a + b$ and the photon survival probability $w = b/c$, and also the volume scattering function $\beta(\varphi)$, which describes the dependence of the scattering intensity on the angle φ between the direction of the scattered ray and the incident ray – the ray incident on an elementary volume. Note that the range of variation of the optical characteristics of sea water is very large: 2–3 orders of magnitude, depending on its chemical-physical composition. If we do not take into account air bubbles in the subsurface water layer, then the optical properties of sea water will be determined by three factors (three optically active components): pure water, dissolved biological substances, and hydrosol suspension. The optical characteristics (coefficients of absorption, scattering, and attenuation and volume scattering function) can be represented as a superposition of the characteristics of the individual components:

$$\sigma_\Sigma = \sigma_{Sc.W} + \sigma_{Abs.W} + \sigma_{Sc.Part.} + C_{ch}\alpha_{ch} + C_y\alpha_y,$$

where $\sigma_{Sc.W}$ and $\sigma_{Abs.W}$ are the scattering and absorption coefficients of pure water, $\sigma_{Sc.Part.}$ is the scattering coefficient of the particles suspended in the water, and C_{ch}, C_y and α_{ch}, α_y are the concentrations and specific absorptions of chlorophyll and yellow substance (dissolved organic matter that has been accumulated in the water over thousands of years). Scattering of light by water molecules obeys Rayleigh's law and is identical for all types of water.

The volume scattering function is an optical parameter that characterizes the scattering particles and determines the process of propagation of radiation in a turbid medium. In the theory of light propagation and remote sensing, a qualitative estimate of the type of a given aqueous medium is provided by various integral parameters of the volume scattering function, such as the average cosine of the scattering angle, the dispersion of the scattering function (the mean square of the scattering angle), the dispersion of the small-angle part of the scattering function, the probability of backscattering (the fraction of light scattered into the backward hemisphere in an elementary scattering act), the probability of scattering into angles $45° \le \gamma \le 180°$, the backscattering coefficient, and the asymmetry factor of the scattering function (defined as the ratio of fluxes scattered by an elementary volume into the forward and backward hemispheres):

$$F_{asym} = \int_0^{\pi/2} \beta(\gamma)\sin\gamma d\gamma \Big/ \int_{\pi/2}^{\pi} \beta(\gamma)\sin\gamma d\gamma .$$

In what follows, we will use the asymmetry factor F_{asym} to describe the scattering function. For natural waters, the values of the asymmetry factor are determined as a first cut by the ratio of the content of the coarse organic fraction and the fine mineral fraction in the hydrosol [16–18].

In our numerical experiments, we use the volume scattering functions $\beta(\varphi)$ and optical interaction coefficients (a, b, c) obtained for fifteen types of sea water by Petzold [17].

RESULTS AND DISCUSSION

The nonstationary radiative transfer equation (Eq. (2)) was solved, implementing the facet model of signal reflection from the wavy surface (Eqs. (3) and (4)), for boundary conditions corresponding to a monostatic lidar (collocated receiver and transmitter). It was assumed that the source and receiver, having fixed dimensions R_s and R_d, respectively, are located in the $Y = 0$ plane of the coordinate system $\boldsymbol{r} = (X, Y, Z)$. It is assumed that the source radiates a Gaussian pulse of arbitrarily set duration in the cone of angles φ_s^i (divergence of the laser beam), and the

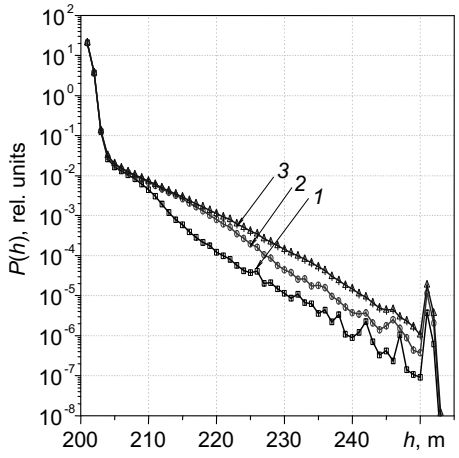

Fig. 1. Dependence of the lidar return signal on distance for receiver field-of-view angles φ_d = 5 mrad (curve *1*), 10 mrad (curve *2*), and 15 mrad (curve *3*). Sea water type P15 [17].

return signal is recorded by a photoreceiver with field-of-view angles φ_d^i = 5, 10, and 15 mrad in the cone $2\pi\left(1-\cos\varphi_s^i\right)$. The altitude of the lidar above the water surface is h_0 = 200 m. The calculations were performed for a wavelength $\lambda = 0.53$ μm (second harmonic of the Nd:YAG laser). We neglect the atmospheric layer located between the receiver and the water surface. Surface wave action was taken into account with the help of the facet model. We assign the wind speed in the interval 0.1–25 m/s. It is assumed that bottom reflection obeys Lambert's law with reflection coefficient 0.1 (a gray bottom). The bottom is located at a depth of 50 m from the water surface. The calculations were performed for unit parameters of the lidar system. In order to convert to actual energy characteristics, it was necessary to multiply the calculated signal values by the area of the receiver telescope, the number of photons in the emitted laser pulse, and efficiency of the entire optical system.

Let us consider a sufficiently simple situation favorable for analysis of the results. The lidar is located at an altitude h_0 = 200 m above the sea surface. The attenuation coefficient of the sea water corresponds to the case P15 in Petzold's classification [17] (a = 0.085 m^{-1}, b = 0.008 m^{-1}, c = 0.093 m^{-1}, and w = 0.086), i.e., the water is very transparent and corresponds roughly to water of the type found in the Coral Sea (Australia). The duration of the laser pulse is 20 ns. The wind speed is 1 m/s. Figure 1 compares calculated return signals for three receiver field-of-view angles φ_{d1} = 5 mrad (curve *1*), $\varphi_{d2} = 10$ mrad (curve *2*), and φ_{d3} = 15 mrad (curve *3*). For such a *simple* situation, the total dynamic range of falloff of the signal comprises 8 orders of magnitude for the minimum field of view (5 mrad), 7.5 orders of magnitude for 10 mrad, and 7 orders of magnitude for 15 mrad. Growth of the multiple scattering fraction is seen in the signal. The initial spike in the intensity out to a depth of several meters is caused by specular reflection from the surface and is equal in duration to the duration of the sensing laser pulse: 20 ns. The dynamic range was estimated from the water surface to the water layer immediately above the bottom. The maximum signal from the bottom exceeds the signal from the above-lying layers of the water column by 1–1.5 orders of magnitude. We subtract out the specular component. In order to do this, we construct an *average curve* for the calculated curves *1*, *2*, and *3* and extrapolate it to the left, to where it intersects the coordinate axis. This happens at the power level $P(h) \approx 10^{-1}$ in relative units, i.e., the dynamic range decreases by approximately 2 orders of magnitude, which substantially reduces the load on the lidar recording system. From this follows the need to use a system to protect from specular glare.

Figure 2 compares calculated return signals for different wind speeds in the range V = 0.1–25 m/s. The attenuation coefficient corresponds to sea water of type P15 in Petzold's classification [17]. The receiver field-of-view angle is φ_d = 15 mrad. Figure 3 plots calculated return signals for waters of type P04 in Petzold's classification [17]. The wind speed is 1 m/s. The bottom reflection coefficient is also 0.1. The photon survival probability w was varied over wide limits. Figure 3 plots results obtained on the assumption that the photon survival probability is equal to

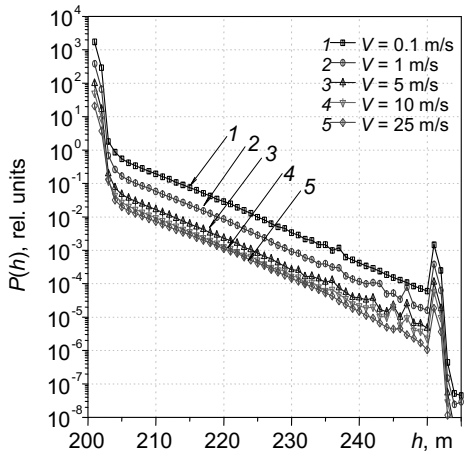

Fig. 2

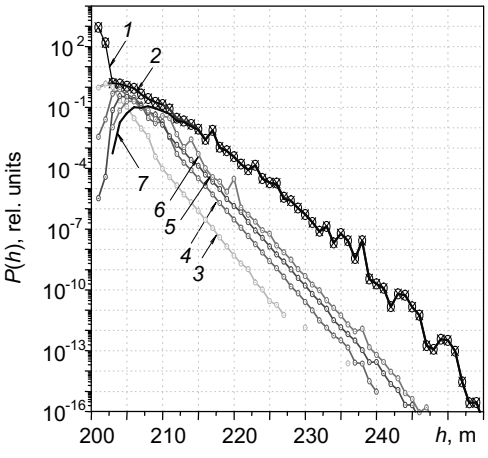

Fig. 3

Fig. 2. Dependence of the return signal on distance for the wind speed $V = 0.1$–25 m/s. Sea water of type P15 [17]. Receiver field-of-view angle $\varphi_d = 15$ mrad.

Fig. 3. Sea water of type P04 [17] for $a = 0.195$ m^{-1}, $b = 0.276$ m^{-1}, $c = 0.47$ m^{-1}, and $w = 0.585$. Receiver field-of-view angle $\varphi_d = 15$ mrad.

0.585: curve *1* corresponds to the total signal, including the scattered signal and the signal reflected from the sea surface, curve *2* corresponds to the total signal due to multiple scattering, curve *3* corresponds to the signal due to the first order of scattering, curve *4* corresponds to the signal due to the second order of scattering, curve *5* corresponds to the signal due to the third order of scattering, curve *6* corresponds to the signal due to the fourth order of scattering, and curve *7* corresponds to the signal due to scattering orders higher than fourth.

The results of our calculations allow us to draw the following conclusions. Confident measurements are possible to a depth of 50 m for water types P02, P14, and P15 in Petzold's classification [17]. Measurements are also possible for water types P03 and P09 [17]. For water types P04, P05, P06, P07, P08, P10, P12, and P013 [17] under these conditions, depth measurements are not possible.

This does not mean that depth measurements are impossible under softer conditions out to the limiting depth for a higher bottom albedo (brighter bottom) and more favorable scattering functions.

On the whole, the possibility of measuring the depth is determined by the optical thickness of the water $\tau = cL$, where c is the attenuation coefficient, and L is the depth of the sensed layer. Thus, the need arises in the process of sensing to measure the attenuation coefficient. This can be done using the return signal of the bathymetric lidar itself. As for the effect of wind speed, one conclusion is obvious from the calculated results: the higher the wind speed, the harder it is to make measurements. The total intensity of the signal from the water column decreases with increase of the wind speed, i.e., with increase of the surface wave heights, but the contrast of reflection from a flat bottom remains practically unchanged.

Measurement of surface wave heights can also be done using the lidar. The average wave height affects the errors in the depth measurements since the reference (mean) level of the sea surface from which the bottom depth is measured can vary.

Calculation of the errors in the depth measurements creates difficulties. First of all, when working in the lidar scanning regime, as the aircraft flies over the given area of the sea surface, at each point in space (one pixel on the bottom) only one radiation signal is incident; therefore, no acceptable statistics are possible. The determining inaccuracies will be assigned only by the total error of determination of the average level of the surface and the error of measurement of the leading edge of the return signal from the bottom.

CONCLUSIONS

By solving the nonstationary equation of laser sensing of a complex, multicomponent, optically dense aqueous medium with allowance for the influence of the water–air interface, the contribution due to multiple scattering by the water column and the contribution due to reflection of the signal from the bottom, we have obtained dependences of the return signal of a monostatic lidar on depth and surface microwaves for different field-of-view angles of the receiver. The results of our calculations show that a bottom detection depth up to 50 m is achievable up to water optical thicknesses of 3.5–4. When sensing the bottom up to the limiting depth of 50 m under conditions of very transparent water and in the presence of Fresnel reflection from the water surface, the dynamic range of the signal from the water column reaches 7–9 orders of magnitude.

REFERENCES

1. H. H. Kim, Appl. Opt., **16**, No. 1, 46–56 (1977).
2. K. Fredriksson, B. Galle, K. Nystrom, *et al*. Underwater laser-radar experiments for bathymetry and fish school detection: Report GJPR-162, Göteborg Inst. Phys., Göteborg (1978).
3. V. S. Shamanaev, I. É. Penner, G. P. Kokkhanenko, and M. M. Krekova, Nauka – Proizvodstvu, No. 9(65), 20–23 (2003).
4. V. S. Shamanaev, I. É. Penner, and M. M. Krekova, Opt. Atmos. Okeana, **22**, No. 7, 681–689 (2009).
5. V. S. Shamanaev, I. É. Penner, M. M. Krekova, *et al*., Russ. Phys. J., **48**, No. 12, 34–39 (2005).
6. V. S. Shamanaev, Russ. Phys. J., **50**, No. 12, 1178–1182 (2007).
7. V. S. Shamanaev, Russ. Phys. J., **56**, No. 7, 813–821 (2013).
8. Feigels V. I., Park J. Y., Aitken J., et al., Proc. SPIE, **8532-48**, 1–10 (2012).
9. V. A. Gladkikh, V. G. Lizogub, G. P. Kokhanenko, and V. S. Shamanaev, Prib. Tekh. Eksp., No. 1, 85–88 (1996).
10. G. I. Marchuk, ed., The Monte Carlo Method in Atmospheric Optics, Springer, Berlin (1980).
11. G. M. Krekov, G. A. Mikhailov, and B. A. Kargin, Russ. Phys. J., **11**, No. 9, 99–105 (1968).
12. B. A. Kargin, G. M. Krekov, and M. M. Krekova, Opt. Atmos. Okeana, **5**, No. 3, 292–299 (1992).
13. A. S. Monin and P. P. Krasnitskii, Phenomena on the Ocean Surface [in Russian], Gidrometeoizdat, Leningrad (1985).
14. G. Cox and W. Munk, J. Opt. Soc. Am., **44**, 833–850 (1954).
15. Yu. A. Mullamaa, Izv. Akad. Nauk SSSR, Ser. Fiz. Atmos. Okeana, **4**, No. 7, 770–775 (1968).
16. O. V. Kopelevich, in: Ocean Optics, Vol. 1, Physical Ocean Optics [in Russian], A. S. Monin, ed., Nauka, Moscow (1983), pp. 166–208, 208–235.
17. T. J. Petzold, Volume Scattering Functions for Selected Ocean Waters, Scripps Institution of Oceanography, Visibility Laboratory, San Diego (1972).
18. V. I. Haltrin, Proc. SPIE, **5544 (**2014); DOI: 10.1117/12.558313.